ChemPubSoc Europe

DOI: 10.1002/batt.201800108

BATTERIES & SUPERCAPS
Articles

Vanadium Oxide Nanosheets for Flexible Dendrite-Free Hybrid Aluminium-Lithium-Ion Batteries with Excellent Cycling Performance

Xuefei Gong,[a] Jingwei Chen,[a] Shaohui Li,[a] Lars Mohrhusen,[b] Katharina Al-Shamery,[b] and Pooi See Lee*[a]

Aluminum (Al)-ion batteries can be an attractive alternative to lithium-ion batteries because of low costs, high volumetric capacities and dendrite-free formation when Al is used as anode. However, there are limited cathode materials for Al-ion batteries that can deliver satisfactory electrochemical performance, especially cycling stability. The major reason for that is the sluggish kinetics of ion intercalation/deintercalation, resulting from large coulombic attraction between Al^{3+} and cathodes. Herein, a concept of hybrid Al–Li-ion batteries is proposed to circumvent the poor Al^{3+} ions insertion/extraction kinetics in Al-ion batteries, and maintain the dendrite-free characteristics of Al-ion batteries. The high volumetric capacity (32.5 mAh/cm^3 at 100 mA/cm^3, based on the total volume of cathode), enhanced rate capability (21.5 mAh/cm^3 at 1000 mA/cm^3) and excellent cycling performance (70.1% retention after 3000 cycles) have been achieved in the hybrid Al–Li-ion battery composed of vanadium oxide nanosheets on carbon fibers as cathode and Al as anode in a mixed [EMIM][Cl]/$AlCl_3$/LiCl electrolyte. Combining with the good flexibility of cathode and anode, the hybrid Al–Li-ion battery maintains structural and capacity stability under different bending angles. This study unveils a safe, cost-effective and flexible hybrid Al–Li-ion battery that presents highly competitive advantages among various energy storage devices.

1. Introduction

Characterized with high energy densities, Li-ion batteries have been rapidly developed and widely adopted as energy storage devices in the last several decades. However, the safety issues of Li-ion batteries, especially short circuit resulting from dendrites, and unsatisfactory power density have driven researchers to look for alternative candidates.[1,2]

Al-ion batteries meet the requirements of safety in energy storage technology due to the absence of dendrites formation and utilization of ionic liquid based electrolyte with wide operating temperature range.[3–5] With the characteristics of low reactivity, Al is the most abundant elements among metals, low cost and can be safely handled, making the metal suited for direct use as anode in the Al-ion batteries, thus eliminating the need of inactive components (like conductive materials, binder and current collector).[4,5] Moreover, high specific capacity (2980 mAh/g) and volumetric capacity (8046 mAh/cm^3) of Al anode can be achieved with its three electrons transfer during the redox reactions (Al/Al^{3+}), which makes Al-ion batteries even more attractive among energy storage devices.[3–5]

Over the past years, tremendous efforts have been devoted to identifying suitable cathode materials for Al-ion batteries.[3–5] Various materials, including carbonaceous materials,[6–10] metal oxides[11–13] and sulfides[14–16] have been investigated. Graphite, consisting of adjacent layers of carbon atoms with large space, is ideal for ion intercalation/deintercalation.[3,8] Dai's group engineered the natural graphitic into 3-D foam structures, thus shortening the diffusion length and facilitating the ion intercalation/de-intercalation.[3] No chemical bonds were formed during the charging/discharging process, resulting in excellent cycling life (7500 cycles without decay) and rate capability at high current densities (100 mA/g–5000 mA/g). However, the critical drawback was the low discharge capacity (~60 mAh/g), similar to other carbonaceous materials, like graphene.[6,7,9,10] Thus, metal oxides and sulphides are being considered for cathode materials in Al-ion batteries. A discharge capacity as high as 350 mAh/g at a current density of 50 mA/g was successfully obtained with nickel sulfide/graphene as cathode materials.[14] However, after 10 cycles, only 28.5% capacity could be retained. When the current density was increased four times at 200 mA/g, the discharge capacity quickly dropped to 235 mAh/g, 67.1% of its original value. Other metal oxides and sulfides also encountered undesirable cycling stability and rate capability issues even though they could possess comparably higher discharge capacities than carbonaceous materials.[11,12,15,16] Similarly, 3D hierarchical CuS@C could only retain 42.5% of its original discharge capacity (240 mAh/g) after 20 cycles and delivered a low discharge capacity of 140 mAh/g at a current density of 150 mA/g.[15] The primary reason is the

[a] X. Gong, J. Chen, Dr. S. Li, Prof. P. S. Lee
School of Materials Science and Engineering
Nanyang Technological University
639798, Singapore
E-mail: pslee@ntu.edu.sg
[b] L. Mohrhusen, Prof. K. Al-Shamery
Institute of Chemistry
School of Mathematics and Natural Sciences
Carl von Ossietzky University Oldenburg
P.O. Box 2503, D-26111 Oldenburg, Germany

Supporting information for this article is available on the WWW under https://doi.org/10.1002/batt.201800108

sluggish kinetics of ion insertion/extraction and diffusion.[4,5] It can be ascribed to the large coulombic attraction between the host materials and trivalent Al^{3+}, thus resulting in the difficulty in deintercalating the trapped Al^{3+} and consequently reduced intercalation sites, giving a lower ion intercalation level and rapid capacity decay. Even at elevated temperature of 50 °C, Mo_6S_8, the typical insertion type materials of batteries, delivered undesirable cycling stability (77% retention after 50 cycles).[16]

In this work, the concept of hybrid Al–Li-ion batteries is proposed, which involves the lithiation/delithiation at the cathode with high kinetics while Al stripping/deposition at the anode without dendrite formation in a mixed [EMIM][Cl]/$AlCl_3$/LiCl electrolyte. The schematic representation of the hybrid Al–Li-ion battery is illustrated in Figure 1. During the discharge

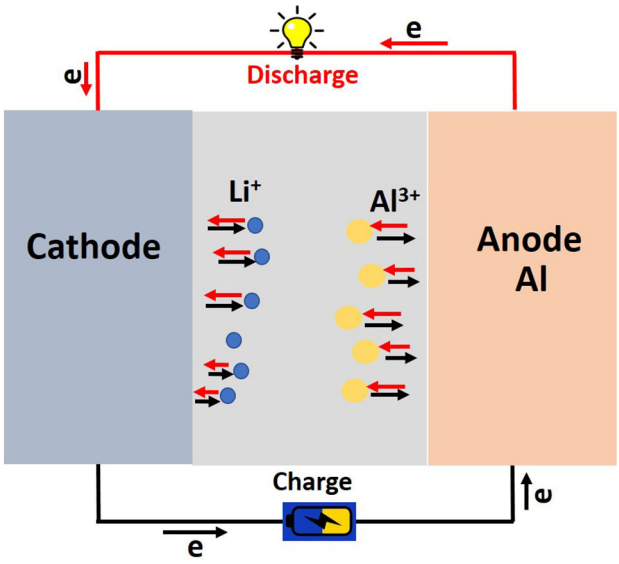

Figure 1. The concept of hybrid Al–Li-ion batteries. The arrows represent the ion movement during charge (black) and discharge (red) processes.

process, Li^+ dominates the intercalation sites in the cathode host materials due to decreased electrostatic interactions between ion and intercalation framework of host materials and lower mass of Li^+ compared to those of Al^{3+}, thus contributing to faster ion mobility compared to the typical Al ion batteries. For the charge process, Al deposition occurs at the anode instead of Li because the thermodynamic redox potential of Al/Al^{3+} (−1.67 V vs. SHE) is 1.37 V higher than that of Li/Li^+ (−3.04 V vs. SHE). This strategy shows great promises in enhancing discharge capacity at high current densities and capacity retention, and circumvents the safety issue from Li dendrite formation at the anode, thus opening an opportunity for the future renewable energy storage applications.

As the typical intercalation compound with layered structures to host ions, vanadium oxide materials are considered one of the most promising electrode materials in energy storage applications because of their high specific capacities originating from multiple valence states, low costs and rich abundance.[11,12,17] However, most vanadium oxides possess inferior electrical conductivity, which leads to sluggish ions and electrons transport and poor rate capability issues. Among them, paramontroseite VO_2 can deliver fascinating electrical properties (1.02 S/cm) due to the presence of infinite chains with shortest V–V distances of 0.293 nm along c axis.[18,19] The short V–V distances enable the d-orbital electrons along c-axis to be shared by all V^{4+} ions. Additionally, paramontroseite VO_2 forms the tunnel framework in which the VO_6 octahedra are linked into double chains and the double chains link corners with each other.[18,19] Owing to the unique tunnel structure and the superior electrical conductivity, the paramontroseite VO_2 can be effective in facilitating the intercalation/deintercalation of ions.

In this work, a flexible, dendrite-free hybrid Al–Li-ion battery was successfully fabricated, comprised of vanadium oxide nanosheets on carbon fibers as cathode and Al foil as anode in a mixed [EMIM][Cl]/$AlCl_3$/LiCl electrolyte. The flexible hybrid battery exhibited a discharge volumetric capacity as high as 32.5 mAh/cm^3 at a current density of 100 mA/cm^3 (based on the total volume of cathode including the substrate of carbon fibers). Even when the current density increased 10 times, a large volumetric capacity of 21.5 mAh/cm^3 could be achieved. More impressively, the capacity retained 70.1% after 3000 cycles. In addition, high flexibility could be obtained as the 3-D porous structure and free-standing design of the electrodes endow the robust structural integrity under mechanical stress. Owing to the novel strategy of the mixed electrolyte and 3D open structures of active materials, the hybrid battery displayed enhanced kinetics of ion diffusion and charge transfer, thus delivering desirable electrochemical performance including high volumetric capacity, enhanced rate capability and excellent cycling stability. This flexible hybrid Al–Li-ion battery offers highly competitive advantages among various energy storage devices.

2. Results and Discussions

Vanadium oxides nanosheets on carbon fibers were synthesized through a simple hydrothermal reaction. It should be mentioned that in the precursors, thioacetamide (TAA) is a sulfur donor in the alkaline conditions and reduces vanadium into the lower valence states. Typically, the product of layered vanadium sulfide (VS_2) nanosheets could be obtained.[20,21] However, due to the strong affinity of vanadium towards oxygen, vanadium sulfide nanosheets with large surface area would undergo fast oxidation process. The nanosheet morphology can be maintained as the oxidation proceeds in a topochemical way.[18,22] The crystallographic structure of our prepared product was identified by X-ray diffraction (XRD) measurements. As shown in Figure 2(a), the typical diffraction peaks of (021) (220) (230) (240) (250) are ascribed to orthorhombic paramontroseite VO_2,[18] in agreement with the JCPDS No. 025-1003. Two other peaks corresponded to tetragonal VO_2 (JCPDS No. 044-0253). Presence of sulfides could not be detected. The morphologies of our synthesized vanadium oxide on carbon fibers were examined using scanning electron microscopy (SEM). From

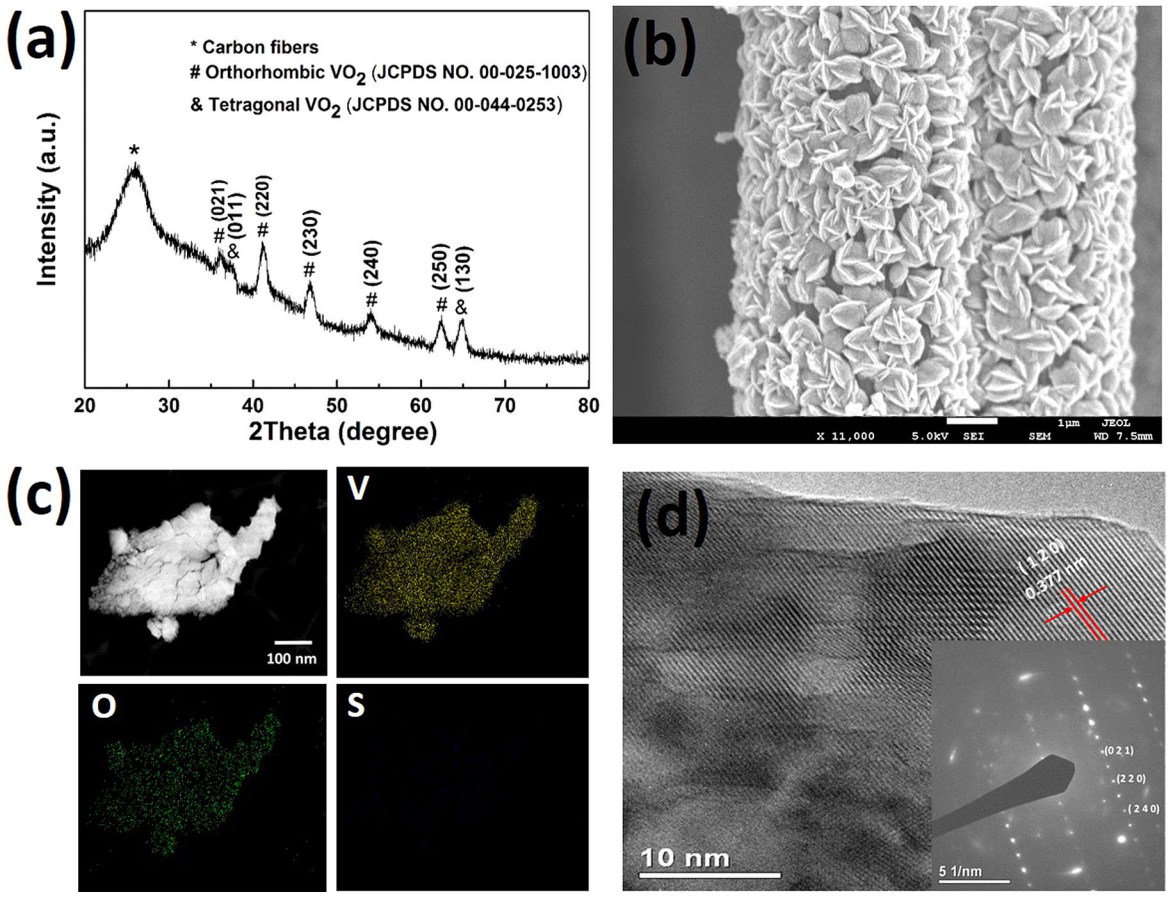

Figure 2. (a) XRD patterns; (b) SEM image; (c) TEM image and the EDS elemental mapping of V, O and S and (d) HRTEM images of the synthesized vanadium oxide on carbon fibers. (The inset on right bottom corner provides the SAED patterns of the sample with planes (021), (220) and (240)).

Figure 2(b) and Figure S1, we can clearly see that vanadium oxide nanosheets (thickness ≈ 30 nm) were vertically grown on carbon fibers. The nanosheets are well-anchored onto the carbon fibers with open configurations providing advantages for electrolyte penetration. Transmission electron microscopy (TEM) was used to further examine our prepared product. Energy-dispersive X-ray spectroscopy (EDS) element mapping (Figure 2(c)) confirms the homogeneous distribution of vanadium and oxygen and the absence of sulfur, indicating the total conversion of vanadium sulfide into vanadium oxide. XPS analysis (Figure S2) also revealed that no sulfur signal could be detected, due to the instability of sulfide, which has transformed into oxides. From the HRTEM image (Figure 2(d)), the lattice d-spacings were measured to be ≈0.377 nm, which is associated with the preferred orientation of (120) crystal planes of orthorhombic VO_2. The selected area electron diffraction (SAED) pattern (inset of Figure 2(d)) also revealed the readily matched orthorhombic VO_2 crystal planes (021), (220) and (240), which further evidenced the formation of paramontroseite in the prepared sample.

To evaluate the advantages of hybrid Al–Li-ion batteries compared to Al-ion batteries, electrochemical performances of two kinds of batteries with vanadium oxide as cathodes were measured and compared. From the CV curves at initial 5 cycles of the full cell hybrid Al–Li-ion battery at the scan rates of 1 mV/s (Figure 3(a)), we can clearly see two cathodic peaks at 0.37 and 0.16 V and two corresponding anodic peaks at 0.7 and 0.38 V. Vanadium oxide (VO_2) is the insertion-type materials in Al-ion and Li-ion batteries[12,17,19] and there is no conversion product. The insertion/extraction mechanism of VO_2 in our hybrid Al–Li-ion battery is also verified. From the ex-situ XRD (shown in Figure S3), we can see the most significant change was the shift of the peak (120) while other peaks maintained almost constant. The peak shift is resulted from ion intercalation and the following structural change.[23] The peak (120) could not shift back after the sample was charged to 0.9 V, due to the trapped ions (irreversible) in the host materials.[23] Thus, the two pairs of peaks correspond to the Li^+/Al^{3+} ions insertion/extraction into/from vanadium oxide structures. It should be noted that the redox peaks did not shift or disappear for the 5 cycles, indicating the highly reversible reactions in the hybrid Al–Li-ion battery. While for the Al-ion battery (Figure S4(a)), one reduction peak at 0.4 V disappeared from the second cycle, suggesting the irreversibility of the electrode. The disappearance of the reduction peak could be attributed to the sluggish kinetics of Al^{3+} ions extraction from intercalation sites of host materials due to the large electrostatic attraction, thus

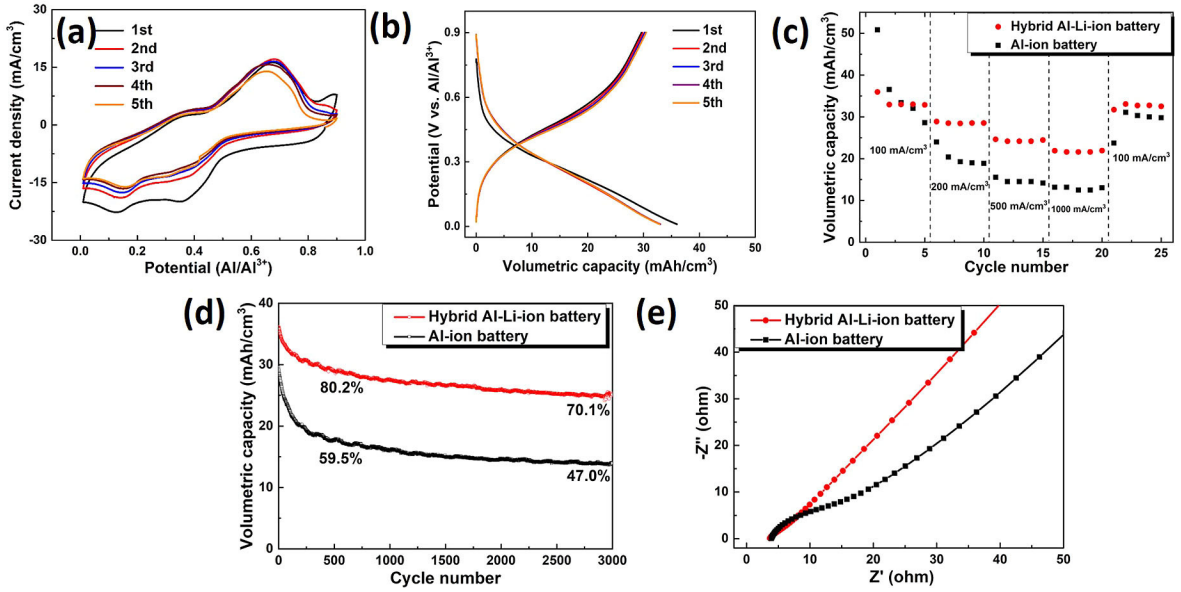

Figure 3. (a) CV curves measured with a potential range of 0.01-0.9 V at a scan rate of 1 mV/s and (b) the first five galvanostatic charging/discharging cycles at a current density of 100 mA/cm^3 of vanadium oxide on carbon fibers as cathode in the hybrid Al–Li-ion battery. (c) Volumetric capacities at different current densities from 100 mA/cm^3 to 1000 mA/cm^3, (d) cycling performance at a current density of 100 mA/cm^3 and (e) EIS measurements at open circuit potential after 5 CV cycles of vanadium oxide on carbon fibers as cathode in hybrid Al–Li-ion battery and Al-ion battery.

the trapped Al^{3+} ions occupied the sites and hindered other Al^{3+} ions from insertion.[16]

The first five galvanostatic charge/discharge (GCD) profiles of the hybrid Al–Li-ion battery and Al-ion battery were also measured as displayed in Figure 3(b) and Figure S4(b). The first discharge and charge volumetric capacity of the hybrid Al–Li-ion battery was 35.9 and 29.6 mAh/cm^3, based on the total volume of cathode, including the vanadium oxide and carbon fibers. It is worth mentioning that the coulombic efficiency of the first charge/discharge cycle for the hybrid Al–Li-ion battery was about 82.3%, much higher compared to that of the Al-ion battery (54.1%). The improved efficiency could be attributed to the decreased electrostatic attraction and enhanced kinetics of ion transport and diffusion. Galvanostatic charge/discharge tests under different current densities were conducted to reveal the rate capability of the hybrid Al–Li-ion and Al-ion battery, as shown in Figure 3(c). With the increase current densities, the volumetric discharge capacities of the hybrid Al–Li-ion battery were notably higher than those of Al-ion battery. Even at a high current density of 1 A/cm^3, the capacity of hybrid Al–Li-ion battery could be maintained at about 21.5 mAh/cm^3, almost 1.5 times higher than that of Al-ion battery. After the current density was brought back to 100 mA/cm^3, the hybrid Al–Li-ion battery restored a capacity of 32.5 mAh/cm^3, still larger than that of Al-ion battery. The enhanced rate capability can be ascribed to the addition of Li^+ ions into the electrolyte that guarantees faster ion transport and diffusion. The cycling stability of the two kinds of batteries were evaluated, as shown in Figure 3(d). It is found that the capacity of Al-ion battery drastically decayed to 59.5% at the initial 500 cycles, which is due to the large electrostatic force of the trapped Al^{3+} ions, thus lowering the ion intercalation level. After 3000 cycles, the capacity retention was about 47.0%. On the contrary, the hybrid Al–Li-ion battery could maintain 80.2% of the original capacity after 500 cycles, then slowly decreased. Finally, the retention could be as high as 70.1% after 3000 cycles. The impressive cycling stability could be attributed to the reduced coulombic attractions between Li^+ ions and vanadium oxide compared to that between Al^{3+} ions and vanadium oxide during repeated ion insertion/extraction. The coulombic efficiency of the batteries were also evaluated. After the activation process of 20 cycles at different current densities, the coulombic efficiency of our hybrid Al–Li-ion battery and Al-ion battery could be enhanced to 98.8% (almost 100%) and 96.1%, respectively, and stabilized for the following 3000 cycles (Figure S5). Such high coulombic efficiencies indicate highly reversible electrochemical reactions. The electrochemical performances of the hybrid Al–Li-ion battery were also compared with other Al-ion batteries. As shown in Table S1, our hybrid Al–Li-ion battery demonstrated the best overall electrochemical performance among the reported Al-ion batteries in terms of capacity, cycling stability and rate capability, revealing the superiority of the hybrid design.

To better explain the improved electrochemical performances, the electrochemical impedance spectroscopy (EIS) spectra of the two kinds of batteries were plotted in Figure 3(e). The intercept of X-axis at high frequencies represents the internal resistance of battery R_s, as shown in the equivalent-circuit diagram Figure S6. It can be clearly seen that both types of batteries delivered similar internal resistances as low as 3.7 Ω. The semicircle at the medium frequency region is associated with the charge transfer resistance at the electrode/electrolyte interface (R_{ct2} in Figure S6). The hybrid Al–Li-ion battery displayed negligible semicircle while the Al-ion battery exhib-

ited the semicircle of ~16 Ω (Figure S7), thus verifying the enhanced charge transfer kinetics of our hybrid battery. It can be explained that introducing one-charge of Li^+ to replace three-charge of Al^{3+} would be beneficial to charge transfer kinetics. The sloping line at the low frequency corresponds to the diffusion behavior of ions (Z_w in Figure S6). The steeper slope line in the hybrid battery reveals the faster diffusion rate than that of Al-ion battery, which is ascribed to the addition of Li^+ ions into the electrolyte. Thus, the hybrid Al–Li-ion battery delivered lower charge transfer resistance, faster diffusion rate and higher ionic conductivity (Figure S8) than those of Al-ion battery, contributing to the improved coulombic efficiency, rate capability and cycling performance.

To illustrate Al^{3+} and Li^+ ions intercalation/deintercalation mechanism in the hybrid Al–Li-ion battery, ex-situ XPS measurements of cathodes were conducted to analyse the V, Al and Li spectra upon the first discharge/charge cycle. In Figure S9, the pristine cathode materials showed the peaks at the binding energies of 516.2 and 523.8 eV of $V2p_{3/2}$ and $V2p_{1/2}$, which could be assigned to V^{4+}.[22,23] To compensate the charge variation, the valence state of vanadium has been decreased with the Al^{3+}/Li^+ insertion during discharge process and increased with Al^{3+}/Li^+ extraction during charge process.[12,23] In the vanadium spectra, when the battery was discharged to 0.3 V, peaks located at 512.1 and 515.1 eV of $2p_{3/2}$, 519.7 and 522.7 eV of $2p_{1/2}$ revealed the existence of V^{2+} and V^{3+}, suggesting the reduction of vanadium during discharging process.[22,23] After the battery continued to discharge to 0.01 V, the disappearance of V^{3+} implied the further reduction of vanadium into V^{2+}. When it was charged to 0.5 V, the oxidation of vanadium could be verified from the new peaks at 517.2 and 524.9 eV, which could be assigned to V^{5+}.[22,23] The increased ration of V^{5+} and V^{4+} peaks illustrated the further oxidation of vanadium after the battery was charged to 0.9 V. The spectra of Li1s and Al2p at 55.6 eV and 74.4 eV could be assigned to Li^+ and Al^{3+}, respectively.[23,24] The XPS peak intensities of Al^{3+} and Li^+ showed no obvious regularity, which could be affected by the residue electrolyte anchored on the cathode materials.[23] However, it should be noted that the intensities of Al2p and Li1s spectra were fluctuated accompanying with vanadium oxidation/reduction during charge and discharge process, respectively, indicating that both Al^{3+} and Li^+ ions were deintercalated/intercalated into the cathode materials, simultaneously. At such a low scan rate of 0.1 mV/s, the Li1s spectra were very weak and noisy, indicating higher amount of Al^{3+} ions intercalation/deintercalation (Figure S9). In contrast, at a high scan rate of 5 mV/s, the Li1s spectra were much smoother and stronger (Figure S10), suggesting that more Li^+ ions participated in the reactions of the cathode materials. This is further supported by the decreased intensity ratio (from 3.45 to 3.34) between Al2p and Li1s at a low scan rate of 0.1 mV/s and a high scan rate of 5 mV/s after the battery was discharged to 0.01 V, indicating that increased percentage of Li^+ ions could be inserted into cathode materials with enhancing scan rates. After the battery was charged to 0.9 V, the intensity ratio between Al2p and Li1s at a low scan rate of 0.1 mV/s and a high scan rate of 5 mV/s also decreased from 3.06 to 1.153, revealing more Al^{3+} ions were trapped into cathode materials at low scan rates. The above-mentioned phenomenon validates the large enhancement of capacities and the improved kinetics of ion insertion/extraction at high current densities.

To further elucidate the enhanced kinetics of our hybrid Al–Li-ion battery, CV analyses were carried out at various scan rates from 0.1 to 100 mV/s to discern the contributions from diffusion-controlled and capacitive behaviour to the total energy storage (Figure 4(a)). The small peak shift among the CV curves in the hybrid Al–Li-ion battery provides evidence of the fast kinetics of charging and discharging process (Figure 4(a)). By contrast, the Al-ion battery displayed severe polarizations at fast scan rates (Figure S11(a)). The power-law relationship between the measured currents (i) and the scan rates (v) was applied to further analyse the kinetics, which is written in Equation (1):

$$i = av^b \tag{1}$$

Where b can be determined from the slope of the plots of log(i) versus log(v) and reflects the electrochemical behaviours. A b-value of 0.5 or 1.0 represents diffusion- controlled or capacitive process, respectively. In the hybrid Al–Li-ion battery, the b values for the cathodic and anodic peaks were 0.93 and 0.76 (Figure 4(b)), respectively, thus indicating the predominant capacitive behaviour and verifying the fast kinetics of energy storage. While in Al-ion battery, the b values were close to 0.5 (Figure S11(b)), suggesting the diffusion-controlled reactions dominate the electrochemical kinetics. To further quantify the capacitive and diffusion-controlled contributions to the total capacity, a method proposed by Dunn and co-workers[25,26] was adopted. In this method, the contribution of capacitive and diffusion-controlled process can be estimated from Equation (2):

$$i = k_1 v + k_2 v^{\frac{1}{2}} \tag{2}$$

Where i is the current (A) at a given potential, v is the scan rate (mV/s) and k_1 and k_2 and are constants. Here $k_1 v$ and $k_2 v^{\frac{1}{2}}$ represent the capacitive behaviour and diffusion-controlled process, respectively. It is observed that in the hybrid Al–Li-ion battery, capacitive behaviour dominated with increasing scan rates (Figure 4(c)). Specifically, at a scan rate of 20 mV/s, 94.4% of capacity was contributed from the capacitive behaviour in hybrid Al–Li-ion battery (Figure 4(c) and (d)), which is much higher than that (80.4%) in Al-ion battery (Figure S11(c) and (d)), suggesting the improved rate capability of the hybrid battery.

To confirm the dendrite-free of the hybrid Al–Li-ion battery, EDX and XRD of Al anode after cycling were measured. As shown in the Figure S12, there were no dendrites on the surface on the Al anode after 3000 cycles. In Figure S14, the typical diffraction peaks of (111) (200) (220) (311) could be assigned to pure Al (JCPDS No. 001-1180), thus further proves the dendrite-free state of our hybrid battery.

In addition to the coin cell fabrication, a fiber-shaped hybrid Al–Li-ion battery was assembled and tested. Fiber-shaped

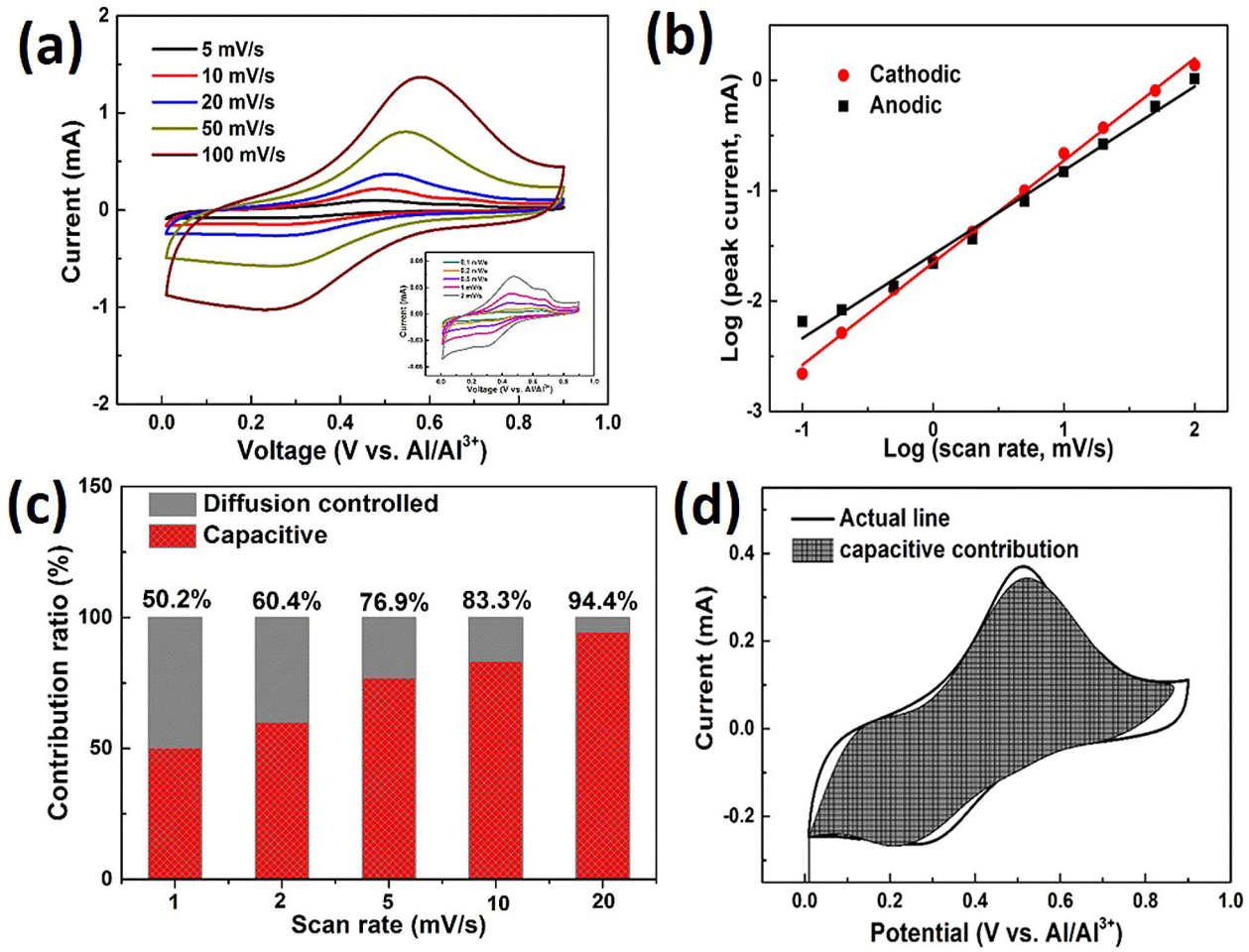

Figure 4. (a) CV curves at various scan rates from 5 to 100 mV/s (inset 0.1 to 2 mV/s), (b) determination of b value through the relationship between peak current and scan rate, (c) capacitive contribution to the total capacity at different scan rates, and (d) estimated capacitive contribution at the scan rate of 20 mV/s in the hybrid Al–Li-ion battery.

energy storage devices are of great interest, as they are light weight, high flexibility and endow shape diversity, which make it applicable in flexible, portable and even wearable applications. As shown in Figure 5, the fiber-shaped hybrid battery can be subjected to bending at different angles without affecting the capacity, indicating good flexibility. The inset of Figure 5 displays two series-connected hybrid Al–Li-ion batteries that could light up a LED. Even at different bending angles, the intensity of the LED light remained the same, revealing good mechanical robustness of the fiber-shaped hybrid Al–Li-ion battery and demonstrating great potential in practical applications.

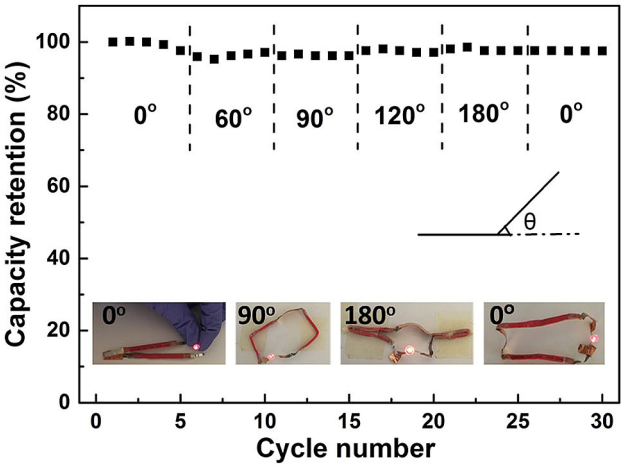

Figure 5. Capacity retention of a hybrid Al–Li-ion battery subjected to different bending angles. (Inset shows two bended Al–Li-ion batteries lit up a LED.)

3. Conclusions

In summary, a flexible dendrite-free hybrid Al–Li-ion battery with vanadium oxide on carbon fibers as cathode and Al as anode was successfully assembled. The intrinsic challenges of dendrite growth in lithium batteries and poor Al ions insertion/extraction kinetics in Al-ion batteries have been simultaneously circumvented in this hybrid design. The hybrid battery presents a reversible capacity of 32.5 mAh/cm^3 (based on the total

volume of vanadium oxide and carbon fibers) at 100 mA/cm^3 and exhibits excellent long-term cycling performance with 70.1% capacity retention for 3000 cycles. Moreover, as the Al foil simultaneously acts as the anode material and the current collector, dead load and dead volume of the battery can be greatly reduced. Therefore, with the merits of safe and cost effectiveness, the hybrid Al–Li-ion battery is attractive and promising for future energy storage applications.

Experimental Section

Synthesis of vanadium oxide nanosheets on carbon fibers as cathode electrode: Carbon fibers (Toray@T1100G) were cleaned with acetone, ethanol and deionized water for several times and dried at 60 °C overnight. Vanadium oxide nanosheets were synthesized through a simple hydrothermal reaction. Typically, 70 mg NH_4VO_3 and 338 mg thioacetamide (TAA) was dissolved into 20 ml DI water and 2 ml NH_3H_2O with continuous magnetic stirring for 1 h at room temperature. After that, the mixed solution was transferred into a Teflon-lined sealed autoclave with capacity of 50 ml. A bundle of carbon fibers (diameter of 4 mm, length of 5 cm) was immersed into the solution as the substrates for the nanosheets growth. The autoclave was sealed and heated at 180 °C for 20 h. After the reaction, the carbon fibers with vanadium oxides nanosheets were rinsed with water and ethanol and dried at 60 °C in vacuum oven for further use as the cathode electrode. The loading mass of vanadium oxide nanosheets on carbon fibers was 1.4 g/cm^3.

Material characterizations: The crystallographic information, chemical states and composition of electrode materials were investigated by X-ray diffraction (XRD, Bruker D8 Advance with the Cu Kα radiation) and X-ray photoelectron spectroscopy (XPS, Thermo-FisherESCALab 250 Xi with monochromatic Al Kα radiation). For the XPS measurements, all spectra were measured using argon assisted charge compensation and were calibrated to C1s peak with a fixed value of 284.4 eV. The pass energies, energy step size, dwell time and the number of iterations for averaging for the specific spectra are 10 eV, 100 ms, 0.05 eV and 10 iterations, respectively. These parameters for the survey are 200 eV, 100 ms, 1 eV and 2 scans. The preparation of the pristine electrode for XPS measurements was conducted as following. The cathode materials vanadium oxide on carbon fibers was firstly assembled into a coin cell aging for two weeks, thus the electrolyte could be fully absorbed into cathode material. Subsequently, the battery was opened and cathode material was taken out and washed with ethanol and dried. The same preparation was conducted for those samples discharged and charged at various voltage for XPS measurements. Residual electrolyte was still left on the cathode materials even though it was washed with ethanol as the electrolyte tend to absorb moisture from air. Finally, the samples were adhered on a carbon tape which was mounted on Al substrate to conduct XPS measurements. The morphology and microstructures of electrode materials were characterized by field-emission scanning electron microscopy (FE-SEM 7600F) and transmission electron microscopy (TEM, JEOL 2010).

Electrochemical measurements: The mixed [EMIM][Cl]/$AlCl_3$/LiCl electrolyte was prepared by adding LiCl into [EMIM][Cl]/$AlCl_3$ (1:1.5, purchased from Sigma-Aldrich) ionic liquid. The mole ratio of Al^{3+}:Li^+ was 3:1. With vanadium oxide on carbon fibers as cathode, Al foil as anode, glass fiber membrane as the separator and the above mixed [EMIM][Cl]/$AlCl_3$/LiCl as electrolyte, a CR2032-type coin cell was assembled in the glovebox ($H_2O < 0.1$ ppm, $O_2 <$ 0.1 ppm) to evaluate electrochemical performance. Cyclic voltammograms (CV) and electrochemical impedance spectroscopy (EIS) were tested on an Autolab electrochemical workstation. CV was measured at various scan rates. EIS was conducted at a frequency ranging from 0.1 Hz to 100 kHz with potential amplitude of 5 mV. The charging/discharging measurements were performed with on a LAND battery testing system (CT2001A). For comparison, an Al-ion battery was assembled in a similar way with [EMIM][Cl]/$AlCl_3$ as the electrolyte without the addition of LiCl. Flexible batteries were fabricated with a thermoplastic tube as the package. All the tests were conducted at room temperature.

Acknowledgements

This project is funded by the Singaporean-German S&T Cooperation Researcher Mobility Scheme (SGP-PROG2-011) and NRF Investigatorship Award NRF-NRFI2016-05. We also thank Prof. Al-Shamery's group for the use of XPS and its analysis. The XPS was supported by the German science foundation (Deutsche Forschungsgemeinschaft) (INST 184/144-1FUGG). Xuefei Gong acknowledges the scholarship awarded by the Nanyang Technological University, Singapore.

Conflict of Interest

The authors declare no conflict of interest.

Keywords: dendrite-free · flexible batteries · hybrid aluminium-lithium-ion batteries · kinetics · nanostructures

[1] J.-M. Tarascon, M. Armand, *Nature* **2001**, *414*, 359.
[2] V. Etacheri, R. Marom, R. Elazari, G. Salitra, D. Aurbach, *Energy Environ. Sci.* **2011**, *4*, 3243.
[3] M.-C. Lin, M. Gong, B. Lu, Y. Wu, D.-Y. Wang, M. Guan, M. Angell, C. Chen, J. Yang, B.-J. Hwang, *Nature* **2015**, *520*, 325.
[4] F. Ambroz, T. J. Macdonald, T. Nann, *Adv. Energy Mater.* **2017**, *7*, 1602093.
[5] G. A. Elia, K. Marquardt, K. Hoeppner, S. Fantini, R. Lin, E. Knipping, W. Peters, J. F. Drillet, S. Passerini, R. Hahn, *Adv. Mater.* **2016**, *28*, 7564.
[6] H. Chen, F. Guo, Y. Liu, T. Huang, B. Zheng, N. Ananth, Z. Xu, W. Gao, C. Gao, *Adv. Mater.* **2017**, *29*, 1605958.
[7] D.-Y. Wang, C.-Y. Wei, M.-C. Lin, C.-J. Pan, H.-L. Chou, H.-A. Chen, M. Gong, Y. Wu, C. Yuan, M. Angell, *Nat. Commun.* DOI: 10.1038/ncomms14283.
[8] H. Sun, W. Wang, Z. Yu, Y. Yuan, S. Wang, S. Jiao, *Chem. Commun.* **2015**, *51*, 11892.
[9] L. Zhang, L. Chen, H. Luo, X. Zhou, Z. Liu, *Adv. Energy Mater.* **2017**, 1700034.
[10] Y. Wu, M. Gong, M. C. Lin, C. Yuan, M. Angell, L. Huang, D. Y. Wang, X. Zhang, J. Yang, B. J. Hwang, *Adv. Mater.* **2016**, *28*, 9218.
[11] H. Wang, Y. Bai, S. Chen, X. Luo, C. Wu, F. Wu, J. Lu, K. Amine, *ACS Appl. Mater. Interfaces* **2014**, *7*, 80.
[12] W. Wang, B. Jiang, W. Xiong, H. Sun, Z. Lin, L. Hu, J. Tu, J. Hou, H. Zhu, S. Jiao, *Sci. Rep.*DOI: 10.1038/srep03383.
[13] N. Jayaprakash, S. K. Das, L. A. Archer, *Chem. Commun.* **2011**, *47*, 12610.
[14] S. Wang, Z. Yu, J. Tu, J. Wang, D. Tian, Y. Liu, S. Jiao, *Adv. Energy Mater.* **2016**, *6*, 1600137.
[15] S. Wang, S. Jiao, J. Wang, H.-S. Chen, D. Tian, H. Lei, D.-N. Fang, *ACS Nano* **2016**, *11*, 469.
[16] L. Geng, G. Lv, X. Xing, J. Guo, *Chem. Mater.* **2015**, *27*, 4926.
[17] P. Liu, K. Zhu, Y. Gao, H. Luo, L. Lu, *Adv. Energy Mater.* **2017**, *7*, 1700547.
[18] C. Wu, Z. Hu, W. Wang, M. Zhang, J. Yang, Y. Xie, *Chem. Commun.* **2008**, *0*, 3891.
[19] C. Wu, Y. Xie, *Energy Environ. Sci.* **2010**, *3*, 1191.

[20] J. Feng, X. Sun, C. Wu, L. Peng, C. Lin, S. Hu, J. Yang, Y. Xie, *J. Am. Chem. Soc.* **2011**, *133*, 17832.
[21] P. He, M. Yan, G. Zhang, R. Sun, L. Chen, Q. An, L. Mai, *Adv. Energy Mater.* **2017**, *7*, 1601920.
[22] Y. Wang, Z. Sofer, J. Luxa, M. Pumera, *Adv. Mater. Interfaces* **2016**, *3*, 1600433.
[23] S. Gu, H. Wang, C. Wu, Y. Bai, H. Li, F. Wu, *Energy Storage Mater.* **2017**, *6*, 9.
[24] X. Liang, Q. Pang, I. R. Kochetkov, M. S. Sempere, H. Huang, X. Sun, L. F. Nazar, *Nat. Energy* **2017**, *2*, 17119.
[25] X. Wang, G. Li, Z. Chen, V. Augustyn, X. Ma, G. Wang, B. Dunn, Y. Lu, *Adv. Energy Mater.* **2011**, *1*, 1089.
[26] Z. Chen, V. Augustyn, X. Jia, Q. Xiao, B. Dunn, Y. Lu, *ACS Nano* **2012**, *6*, 4319.

Manuscript received: October 14, 2018
Revised manuscript received: November 28, 2018
Accepted manuscript online: December 19, 2018
Version of record online: January 23, 2019